

# Dielectrophoresis in aqueous suspension: impact of electrode configuration

Y. Wang · F. Du · M. Baune · J. Thöming

Received: 10 September 2013 / Accepted: 20 December 2013 / Published online: 3 January 2014  
© Springer-Verlag Berlin Heidelberg 2014

**Abstract** Dielectrophoresis (DEP) allows to moving neutral or charged particles in liquids by supplying a non-uniform electric field. When using alternating current and insulated electrodes, this is possible in conducting media such as aqueous solutions. However, relatively high field strength is required that is discussed to induce also an undesired Joule heating effect. In this paper, we demonstrate boundary conditions for avoiding this side effect and suggest a novel design of an interdigitated electrode (IDE) configuration to reduce the power consumption. Numerical simulation using OpenFOAM demonstrated that, when replacing conventional plate IDE by cylindrical micro-IDE in microchannel systems, the dielectrophoretic force field, i.e., the electric field gradient squared, becomes stronger and more homogeneously distributed along the electrodes array. Also the resulting particle DEP velocities were highest for the cylindrical IDE. The simulations were experimentally confirmed by measuring velocity of resin particle located at the subsurface of demineralized water. Surprisingly the fluid flow induced by electrothermal effect turned out to be negligible in microchannels when compared to the DEP effect and becomes dominant only for distances between particle and IDE larger than 6,000  $\mu\text{m}$ . The well-agreed experimental and simulation results allow for predicting particle motion. This can be expected to pave the way for designing DEP microchannel separators with high throughput and low energy consumption.

**Keywords** Dielectrophoresis · Electric field gradient · Interdigitated electrode · Numerical simulation · Particle velocity in aqueous suspension

## Abbreviations

AC	Alternative current
CCD	Charge-coupled device
CFD	Computational fluid dynamics
DC	Direct current
DEP	Dielectrophoresis
eff	Effective
ETE	Electrothermal effect
EFG	Electric field gradient squared
$F_{\text{DEP}}$	Dielectrophoretic force
IDE	Interdigitated electrode configuration
nDEP	Negative DEP
pDEP	Positive DEP
$\text{re}[\tilde{K}]$	Real part of the Clausius–Mossotti factor
rms	Root mean squared

## 1 Introduction

Dielectrophoresis (DEP), a translational motion of suspended particle induced by dielectric polarization in an inhomogeneous electric field, was firstly defined by Pohl (1978). In contrast to electrophoresis, DEP is not limited to direct current, it acts on both neutral and charged particles, and it can lead to higher particle velocities with identical voltage input (Thöming et al. 2006).

DEP is already widely applied in such areas as biosensors, cell therapeutics, medical diagnostics, and

Y. Wang · F. Du (✉) · M. Baune · J. Thöming  
UFT, Center for Environmental Research and Sustainable  
Technology, University of Bremen, Leobener Straße,  
28359 Bremen, Germany  
e-mail: feidu@uni-bremen.de

nanoassembly. As a new separation technique, DEP is attracting more and more interest for fractionating, and concentrating micro- and nanoparticles in microfluidic systems (Jones 1995; Pethig and Markx 1997; Green et al. 1997; Morgan and Green 2003; Baune et al. 2008; Du et al. 2013; Pethig 2010; Khoshmanesh et al. 2011; Cetin and Li 2011) with maximum flow rates of the order of milliliters per minute and electrode distances in the micrometer range (Li et al. 2010; Srivastava et al. 2011).

First attempts in scaling-up DEP separations followed the approach to enlarge the diameter of the flow channel and thereby electrode distance. Baune et al. (2008) experimentally investigated DEP systems with electrode distances in millimeter scale and described the Joule heating challenge attributed to the correspondingly low volumetric surface. Du et al. (2008) followed the same approach developing a DEP particle separator for fractionating gold particles from an aqueous suspension of heavy minerals with 141 mL/min throughput. Sano et al. (2012) proposed a dielectrophoretic particle separator using three-dimensional mesh stacked electrodes to separate tungsten carbide particles from a mixture with diatomite. Cetin and Li (2011) emphasized the rarity of research on the improvement of throughput of DEP system, for replacing the benchtop instruments of microfluidics for clinical applications.

For continuous separation, fluid flow has to be split into two or more streams. The bigger the difference achieved in particle concentrations of these streams, the higher the separation factor. This in turn depends on particle trajectories, which result from two superimposed forces, the dielectrophoretic force and the drag force. While the latter is determined by fluid flow, the dielectrophoretic force field can be described by the electric field gradient squared (EFG). According to Pohl (1978), EFG can be expressed as  $((E \cdot \nabla)E = \frac{1}{2} \nabla |E|^2)$ , in case of linear and isotropic dielectrics. As an example, Pohl described the (geometric) EFG in a cylindrical electrode configuration by:

$$\nabla |E|^2 = \frac{-2U_m^2}{r^3 \left( \ln \left( \frac{r_1}{r_2} \right) \right)^2} \quad (1)$$

where  $E$  is the electric field intensity,  $U_m$  is the voltage across medium,  $r$  is the distance between particle and electrode,  $r_1$  is the radius of central electrode, and  $r_2$  is the characteristic length of electrode configuration. Thus, magnitude and distribution of EFG depend on both voltage input and structure parameters of electrode configuration.

According to the relationship between particle trajectories on the one hand and electrode configuration and fluid flow direction on the other, electrode arrangement in the flow channel is a key element of a DEP separator. Principally there are two options, orthogonal and horizontal

arrangement. In the orthogonal electrode arrangement (Fig. 1a), two electrodes are oppositely installed on two sides of the channel with fluid flowing in between both electrodes. Differently, in the horizontal electrode arrangement (Fig. 1b), electrodes are installed on one side of channel and the fluid passes them subsequently. Typically the horizontal electrode arrangement is realized as an array. This is called interdigitated electrode configuration (IDE) and already utilized in DEP microsystems such as chips for particle separation (Weiss et al. 2009; Kumar et al. 2009; Morganti et al. 2011).

On the other hand, the increase in fluid flow will require much higher electric field input for generating sufficiently high DEP force to effectively move particles.

An increase in throughput can be achieved by an increase in particle concentration and fluid flow rate. In case of orthogonal electrode configuration, an increase in particle concentration enhances the interaction between particles, which possibly align along the electric field forming a chain-like agglomeration of particles. This pearl-chain effect (Jones 1995) might intervene in DEP motion and potentially bridge the two electrodes. Such a “short-circuit” between electrodes will increase electrical current and thus energy consumption of the DEP system (Du et al. 2009). In case of large particles forming chains, the open cross-sectional area of the channel is reduced and so is the DEP effect due to increased fluid velocity.

To realize a certain EFG with an orthogonal electrode configuration, a relatively high voltage is required in comparison with an IDE due to the relative large distance between electrodes. Concurrently, for a certain voltage input in a DEP system, the DEP force can be enhanced cubically by decreasing the distance between electrodes.

Currently, the IDEs applied in DEP systems are configured with metal plates (either insulated or bare). The disadvantages of such a plate IDE system are a very weak electric field at the center of the electrodes and a rapid change of electric field gradient at positions in the vicinity of electrodes (Crews et al. 2007; Cao et al. 2008). Due to both problems, current plate IDE cannot homogeneously manipulate particle trajectories. For this purpose, a novel design of a horizontal electrode configuration is required, which provides a strong electric field gradient that is as homogeneously distributed in the vicinity of electrodes array as possible.

In this paper, we present such a novel design of an IDE configuration that meets the above-mentioned requirements by using cylindrical instead of plate electrodes. We simulated the effect of this decisive modification in terms of electric field gradient squared using OpenFOAM and particle velocity using MATLAB. The results were compared with experimental measurements in a DEP cell.

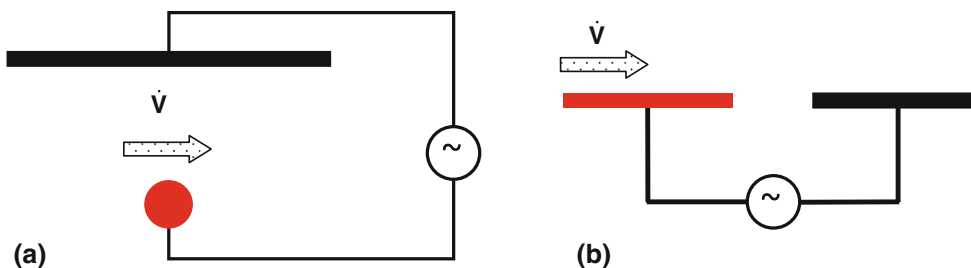


**Fig. 1** Types of DEP electrode configuration: **a** orthogonal and **b** horizontal to the medium flow ( $\dot{V}$ ) with respect to electrode arrangement

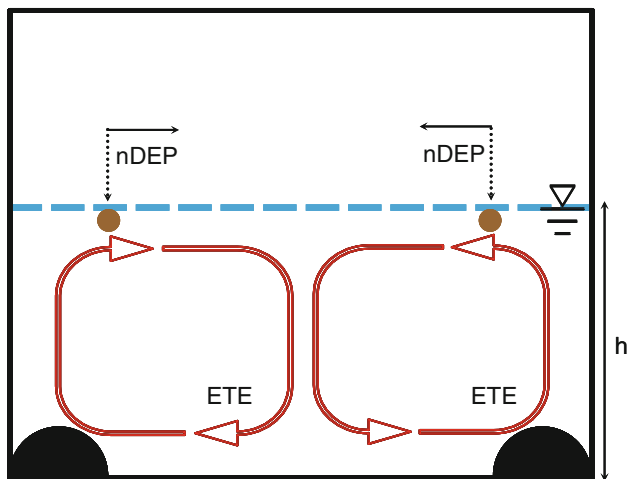


**Fig. 2** Cutout of an IDE-DEP microsystem showing two electrodes (black solid semi-circles) interdigitatedly installed. Particles (brown solid circles) sticking to the subsurface of aqueous medium, which are positioned as indicated by dashed lines, will be moved to mid between two electrodes when an nDEP effect is presented. The resulted fluid flow (red lines) due to electrothermal effect (ETE) will enhance particle motion velocity in the case of nDEP (color figure online)

**2 Materials and methods**

**2.1 DEP system**

The IDE–DEP systems consist of a DEP cell mounted with group of cylindrical IDEs. Suspended particles located at the subsurface of medium will be repelled along horizontal direction under the influence of DEP force from higher electric field region (their initial positions as indicated in Fig. 2), while electrothermal-induced cycling fluid flow follows nDEP force direction (Fig. 2).

**2.2 Experimental setup**

The experimental setup was composed of a CCD camera (IMAGING SOURCE Co. Ltd DFK 31AU03), a lens (IMAGING SOURCE Co. Ltd), a function generator (VOLT CRAFT® 7202) and a power amplifier (FM1290, FM ELEKTRONIK BERLIN). Four electrodes were installed subsequently in a DEP cell (Fig. 2), having

aspect ratio (a ratio of diameter or length of electrode to distance between electrodes,  $d:L$ ) of 1:2. Titanium wires insulated with rutile were used as electrodes with a diameter of 2,000  $\mu\text{m}$ . Insulation on cylindrical electrodes is applied to diminish problems in conductive aqueous media such as the risk of short circuit and electrochemical reaction. Resin particles (with relative dielectric constant of 3) were utilized in the experiment with a mean particle diameter of 808  $\mu\text{m}$ . By settling heavy resin particles in aqueous suspension, a light fraction of particles was obtained that stuck to the surface of the suspension. These collected particles were used in the dielectrophoresis experiment. Both size and velocity of observed single particles were measured. This was done by analyzing the image of particle captured by optical system (CCD camera and lens) and using SigmaScan Pro 5.0, calibrated with standard 500  $\mu\text{m}$  polymer microspheres (Duke Scientific Co. Ltd).

**2.3 Experimental determination of particle velocity**

Due to the much lower permittivity of resin particle compared to that of demineralized water, the resin particle suspended at the water surface presents a negative DEP effect and hence moves toward lower electric field region. The local particle velocity in horizontal direction  $v_x$  was obtained by dividing motion distance ( $\Delta s_x$ ) by motion time ( $\Delta t$ ).

$$v_x = \frac{\Delta s_x}{\Delta t} \tag{2}$$

The initial position of particle is shown in Fig. 2 for exerting the maximum DEP force. Particle velocities were determined at different heights  $h$  (2,000, 2,500, 3,000, 5,000 and 7,000  $\mu\text{m}$ ) above electrodes. Each experiment was repeated 10 times. The height of particle away from electrodes was varied by controlling the height of demineralized water. After experiment, the recorded video clips were processed by capturing pictures using software of SigmaScan Pro. 5.0. The time difference between two captured pictures is chosen in the magnitude of 1/30 s for reducing measurement error at most.

## 2.4 Modeling

Basis for any modeling of DEP is the dependence of direction and magnitude of dielectrophoretic force  $F_{\text{DEP}}$ , which acts on a spherical particle, on the electric field intensity  $E$ , its gradient, effective polarizability and the particle radius. According to Pohl (1978), this writes as:

$$F_{\text{DEP}} = 4\pi a^3 \varepsilon_0 \varepsilon_M \text{re}[\tilde{K}](E \cdot \nabla)E \quad (3)$$

where  $\varepsilon_0 = 8.854 \times 10^{-12} \text{ F m}^{-1}$  is the permittivity of free space,  $\varepsilon_M$  is the permittivity of the medium, and  $\text{re}[\tilde{K}]$  is real part of the Clausius–Mossotti factor  $\tilde{K}$ . This parameter describes the effective dielectric polarizability of the particle as a function of frequency of the electric field and is given as:

$$\text{re}[\tilde{K}] = \text{re}\left(\frac{\tilde{\varepsilon}_P - \tilde{\varepsilon}_M}{\tilde{\varepsilon}_P + 2\tilde{\varepsilon}_M}\right) \quad (4)$$

$$\tilde{\varepsilon} = \varepsilon - \frac{j\sigma}{\omega} \quad (4a)$$

where  $\tilde{\varepsilon}$  is the complex permittivity of the particle ( $\tilde{\varepsilon}_P$ ) and the medium ( $\tilde{\varepsilon}_M$ ),  $\sigma$  is the conductivity,  $\omega$  is the angular frequency of the applied electric field ( $\omega = 2\pi f$ ) in which  $f$  is frequency, and  $j = \sqrt{-1}$ . As shown in Eqs. (3) and (4), the direction of DEP force is dependent on the difference of polarizability between particle and medium. Thus, the DEP force induces a particle motion toward either stronger electric field region, termed as positive DEP (pDEP), or toward weaker electric field region, presenting negative DEP (nDEP).

As the magnitude of DEP force is proportional to EFG, the main challenge in generating sufficient DEP force with low energy consumption is to design electrode systems which avoid the need of large electric potentials to generate a sufficiently high EFG.

The motion of a particle suspended in an aqueous medium under the influence of DEP effect is always assumed to be a steady state by balancing the dielectrophoretic force and the drag force. Thus, the DEP velocity of particle,  $v_{\text{DEP}}$ , can be expressed as:

$$v_{\text{DEP}} = \frac{2a^2 \varepsilon_0 \varepsilon_M \text{re}[K](E \cdot \nabla)E}{3\eta_M} \quad (5)$$

where  $\eta_M$  is the dynamic viscosity of the medium (Morgan and Green 2003).

In Eq. (5), the medium is considered to be static, but this is typically not the case. The electric current causes Joule heating, which in turn leads to a motion of fluid medium induced by temperature gradients (Castellanos et al. 2003), as shown in Fig. 2. Du et al. (2007) developed a model to distinguish between DEP and such a convective fluid flow of velocity  $u$  that is driven by a buoyancy force and increases with Joule heating.

$$u = U_m \sqrt{\frac{\alpha g l^3}{V C_P \eta_M R}} \quad (6)$$

Here  $\alpha$  is volume expansion coefficient,  $g$  is the gravitational acceleration,  $l$  is the characteristic length of the electrode configuration,  $V$  is volume of medium,  $C_P$  is the specific heat capacity of the medium,  $\eta_M$  is the dynamic viscosity of the medium, and  $R$  is the electric resistance of the system.

Both DEP and ETE act on suspended particles. Taking this into account, Eqs. (5) and (6) could be combined to express the velocity  $v$  of the particle motion,

$$v = \frac{2a^2 \varepsilon_0 \varepsilon_M \text{re}[K](E \cdot \nabla)E}{3\eta_M} \pm U_m \sqrt{\frac{\alpha g l^3}{V C_P \eta_M R}} \quad (7)$$

In Eq. (7), the second term represents the motion of medium. In case of pDEP, the medium motion decreases the velocity of suspended particle, while for nDEP, the opposite is the case (Du et al. 2007).

## 2.5 Numerical simulation

Two cases were investigated: for comparing cylindrical IDE with plate IDE configuration, EFG distribution was simulated at microscale, in which both the diameter of electrode ( $d$ ) and the distance between electrodes ( $L$ ) are  $10 \mu\text{m}$  in a DEP system with height ( $h$ ) of  $50 \mu\text{m}$ . In another case, to demonstrate the performance potential of cylindrical IDE, simulations were performed at milliscale with an aspect ratio of 1:2 (electrode diameter of  $2,000 \mu\text{m}$  and distance between electrodes  $4,000 \mu\text{m}$ ).

Simulations were performed by implementing the model into the source code of OpenFOAM, an open-source software package that uses CFD solvers based on the finite volume method. For describing the quasi-electrostatic field, Maxwell's equations were used in the following form (Green et al. 2002):

$$E = -\nabla\phi \quad (8)$$

$$\nabla \cdot J + \frac{\partial \rho}{\partial t} = 0 \quad (9)$$

$$\nabla \cdot (\varepsilon_0 E) = \rho \quad (10)$$

where  $\phi$  is the electric potential,  $\rho$  is the free charge density, and  $J$  is the conduction current. For a homogeneous medium, (8), (9), and (10) can be simplified to Laplace's equation (Ramos et al. 1998):

$$\nabla^2 \phi = 0 \quad (11)$$

Simulations were performed for the two-dimensional plane located at the center line ( $y = Y/2$ ), as presented in Fig. 3. By this means, wall effects and disturbances by the edges

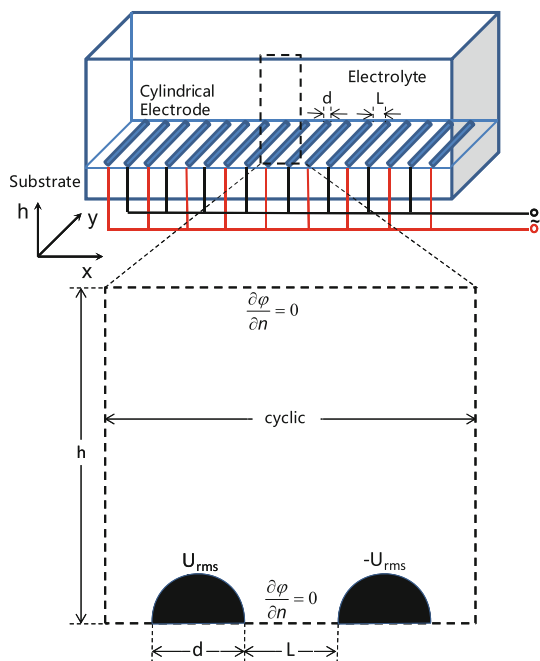


**Fig. 3** Schematic diagram of cylindrical IDE electrode configuration in a rectangular test channel with appropriate boundary conditions

of the electrodes can be neglected since the electrodes are long compared to their diameter. Besides, the periodical array of electrodes allows simplification of the whole system using one representing group of electrodes for simulation (Cao et al. 2008). Further, both alternating current (ac) input voltage and direct current (dc) voltage, equivalent to the root mean squared voltage ( $U_{rms}$ ) of the ac input, were applied. The electric potentials on both surfaces of electrodes were given as positive and negative with a value of  $U_{rms}$ , respectively. On the left and right sides of model, *cyclic* boundary conditions were set to simulate the presence of an infinite number of electrode groups. For the upper and bottom edges between electrodes, either Dirichlet boundary condition ( $\varphi = 0$ ) or Neumann boundary condition ( $\frac{\partial\varphi}{\partial n} = 0$ ) was used with the assumption that the substrate and the top of the chamber always have much lower conductivity and permittivity than the medium in IDE channel (Green et al. 2002).

### 3 Results and discussion

#### 3.1 Comparison of cylindrical IDE and plate IDE

The electric field gradient squared generated by cylindrical IDE was compared with EFG of plate IDE (Fig. 4). The maximum EFG of plate IDE ( $2.16 \times 10^{19} \text{ V}^2/\text{m}^3$ ) at the edges of plates is much higher compared to the maximum value ( $2.8 \times 10^{16} \text{ V}^2/\text{m}^3$ ) of cylindrical IDE at both sides

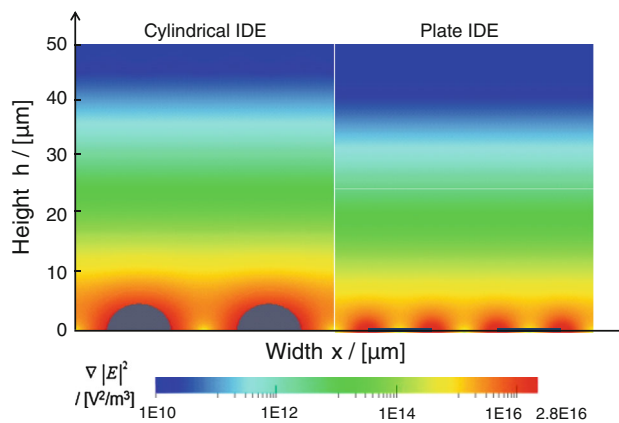


**Fig. 4** Simulation of electric field gradient squared for cylindrical IDE (left) and plate IDE (right). Both the length and diameter of electrodes and the distance between two electrodes were  $10 \mu\text{m}$  (aspect ratio  $d:L = 1:1$ ). The effective voltage applied in this simulation was 1 V

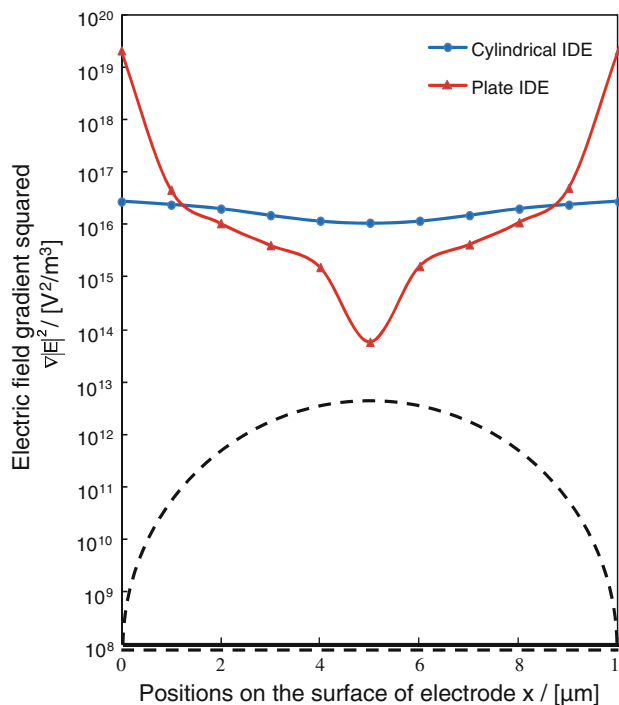


**Fig. 5** Electric field gradient squared distribution on the surfaces of both cylindrical (diameter  $10 \mu\text{m}$ ) and plate IDEs (width  $10 \mu\text{m}$ )

of the cylindrical electrode in the direction of x-axis. Close to the electrodes, the EFG distribution generated by cylindrical electrodes is almost ideally homogeneous, while the extreme EFG values on the plate IDE surface differ for about 6 orders of magnitude (Fig. 5). In addition, the cylindrical IDE has no such areas of very weak EFG around the electrodes, hence improving much larger effective DEP force field area compared to the plate IDE. Further, the EFG of plate IDE shows much smaller values



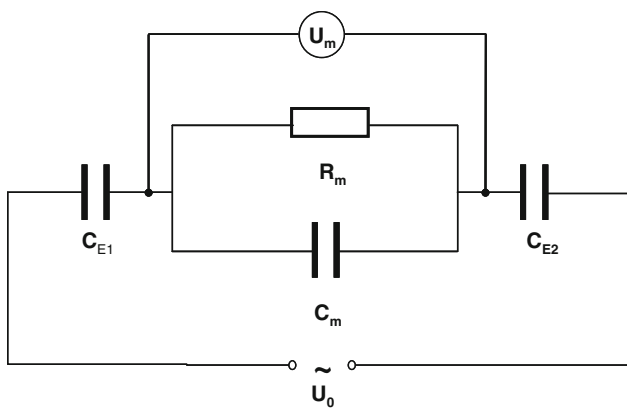


**Fig. 6** Electrical circuit analogy for high-pass-filter effect in an electrode configuration with two electrodes insulated. The dielectric insulation films together with electrode and medium form two capacitors  $C_{E1}$  and  $C_{E2}$ , while the aqueous medium in the electrode configuration can be represented by paralleled connected resistor  $R_m$  and capacitor  $C_m$

than that of cylindrical IDE at the same height of DEP channel. All of these significant improvements from the cylindrical IDE suggest it as promising electrode design for realizing effective DEP effect with lower energy requirement.

Models and simulation were validated by comparison with numerical simulation results from literature (Green et al. 2002) for IDE plate electrode with high consistency in the maximal value and distribution of EFG. However, the mesh resolution influenced the simulation results, and thereby arising mesh error (Visser et al. 2012). The mesh error becomes more significant at the geometrical spots with maximal and minimal gradient terms, but negligible at other positions. The solution from the finer mesh was compared with those from the coarser mesh. It is indicated that a large increase in mesh resolution turns out to be a significant enhancement of maximum value of the electric field gradient squared. The difference of variety of simulation results at the maximal and minimal spots becomes negligibly small, when the mesh resolution reaches a sufficiently high magnitude, which is considered to be the critical fine mesh resolution allowing accurate simulation.

### 3.2 Experimental validation

For DEP application in polar solvents such as aqueous solutions, short circuits as well as electrochemical reactions (electrode fouling) often occurs at bare electrodes and also a reduction in electric field strength across the aqueous solution due to its high conductivity. For avoiding the above-mentioned problem, electrodes need to be insulated. However, the insulated electrodes together with the conductive aqueous medium generate a high-pass filter effect (Baune et al. 2008). It can be represented by an electrical

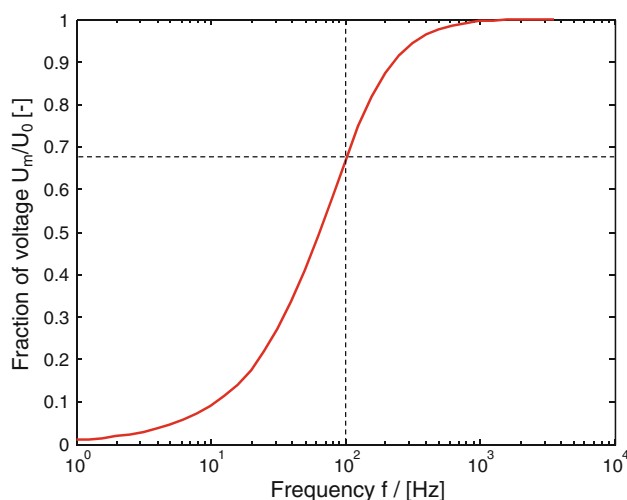


**Fig. 7** Frequency dependence of voltage fraction with aspect ratio ( $d:L$ ) of 1:2. The dashed line indicates the voltage across aqueous medium (electric conductivity of 0.001 S/m) among electrode configurations at the frequency of 100 Hz

circuit as shown in Fig. 6. The capacitors,  $C_{E1}$  and  $C_{E2}$ , formed by dielectric insulation film together with electrodes and aqueous medium, connect in series with parallel connected resistor,  $R_m$ , and capacitor,  $C_m$ , from aqueous medium.

The frequency-dependent voltage fraction, i.e., voltage across the medium  $U_m$  relative to applied voltage  $U_0$ , can be given (Baune et al. 2008),

$$\frac{U_m}{U_0} = \frac{Z_m}{(Z_{E1} + Z_{E2} + Z_m)} \tag{12}$$

where,  $Z$ , impedance formed by insulation films and medium with subscripts of E1, E2 and  $m$ , respectively, can be obtained from,

$$Z_m = \frac{j\omega R_m C_m}{R_m + j\omega R_m C_m} \tag{13}$$

$$Z_{E1} = \frac{1}{j\omega C_{E1}} \tag{14}$$

$$Z_{E2} = \frac{1}{j\omega C_{E2}} \tag{15}$$

In this work, the voltage fraction for electrode configuration with aspect ratio of 1:2 was simulated as shown in Fig. 7. The output voltage  $U_m$  can be obtained as 121.1  $V_{eff}$ , while the applied voltage is 183.5 V at the frequency of 100 Hz.

The transformation of magnitude of cylindrical IDE channel from micrometer to millimeter was performed and verified to be reasonable with sufficient accuracy in simulation, by experimental results as shown in Fig. 8.

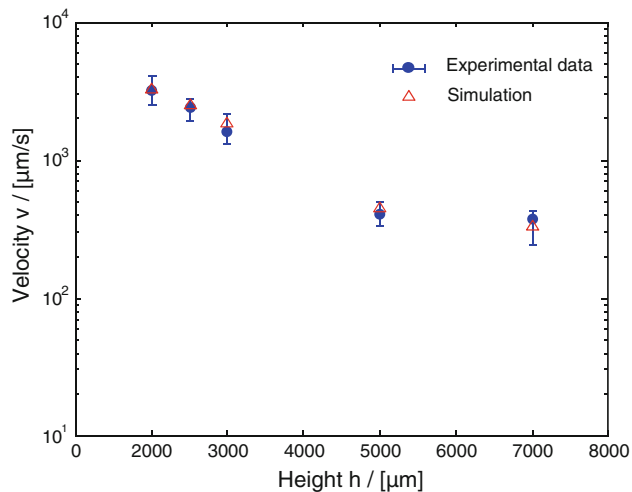


**Fig. 8** Comparison of experimental results of particle velocities and numerical solution using Eq. 7 for different distances between particle and IDE (height  $h$ ) with aspect ratio ( $d:L$ ) of 1:2

The dependency of DEP effect on EFG was experimentally examined by measuring particles motion velocity at different height to the electrodes of a DEP cell and comparing with simulation results. A resin particle suspended at the surface of demineralized water of height  $h$  in the system was observed to move from an electrode (higher electric field region) to the mid between electrodes (lower electric field region) under isothermal conditions ( $T = 298.15$  K), presenting negative DEP effect, as presented in Fig. 2. With rising temperature gradients, an ETE effect was observed with a flow direction from electrode to the mid between electrodes at the surface of aqueous medium, which in turn increased particles motion velocity. Based on the simulation results of EFG in the horizontal direction and using Eq. 7, the velocity of resin particle (diameter of  $808 \mu\text{m}$ ) was theoretically predicted in steady state (Fig. 8). Both simulation results and experimental measurement present high agreement. The experimental error can be estimated by comparing the measured particle motion distance and the half of the characteristic length ( $L/2$ ). The errors for particle motions with maximum velocity and minimum velocity are 5.3 and 0.62 %, respectively.

The influence of ETE on particle DEP effect can be represented by comparing both velocities induced by DEP and ETE, i.e., a ratio of DEP to ETE velocity. The results simulated (Fig. 9) using the identical DEP system in the experiment demonstrated dominant DEP effect, when the particle is positioned very close to the electrodes (lower height to electrodes), where the EFG is higher. As an example, the induced DEP velocity at the height of  $1,000 \mu\text{m}$  to the electrode is about 60 times higher than ETE velocity, as presented in Fig. 9. An equivalent height, at which a balanced effect between DEP and ETE is

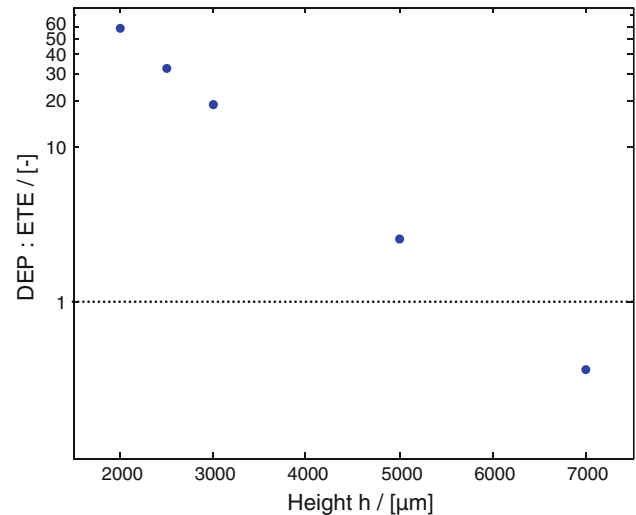


**Fig. 9** Ratio of DEP to ETE velocity at different distances between particle and IDE (height  $h$ ) with aspect ratio ( $d:L$ ) of 1:2

reached, can be obtained. In this DEP system, the equivalent height is  $6,000 \mu\text{m}$ . Above this height, ETE is more dominant. Due to the convective fluid flow induced by the ETE, the particles motion will be disturbed and thereby unpredictable. It demonstrates that a working height of DEP force in a certain IDE–DEP system can be predicted and should be taken into account during design of DEP system, for achieving an effective DEP effect while minimizing the influence of ETE effect.

For studying the impact of electrode configuration to the DEP effect, the DEP velocities of particle at different height ( $1,000$  to  $5,000 \mu\text{m}$ ) to the electrode in three different types of electrode configurations, plate IDE, cylindrical IDE and orthogonal electrode configuration, were simulated as presented in Fig. 10. Both plate and cylindrical electrodes have identical aspect ratio 1:2, i.e., diameter or length of electrode is  $2,000 \mu\text{m}$  with electrodes distanced  $4,000 \mu\text{m}$ . The distance between electrodes in the orthogonal electrode configuration is  $4,000 \mu\text{m}$ , while the diameter of smaller spherical electrode is  $2,000 \mu\text{m}$  with another plate electrode oppositely positioned above it at a distance of  $6,000 \mu\text{m}$ , as shown in Fig. 1a. Hence, in the case of orthogonal electrode configuration, the maximal height of particle position is the electrodes distance. The variety of DEP velocity as a function of height presents a similar tendency, which is the decrease in DEP velocity with the increase in height. The cylindrical IDE generates much higher (around 3.3 times to plate IDE and 2.9 times to the orthogonal electrode in average) DEP velocity compared to the others, due to its more inhomogeneous electric field induced by the more non-uniformly structured electrode configuration. It hints that the cylindrical IDE could provide similar DEP effect at the same height to the electrodes but requiring much lower voltage input, thereby

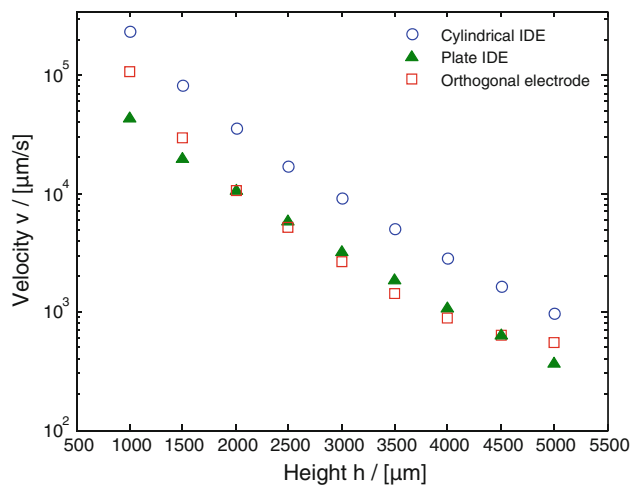


**Fig. 10** Simulation comparison of DEP velocity (logarithm) at different distances between particle and IDE (height  $h$ ) in cylindrical IDE, plate IDE, and orthogonal electrode configuration with identical voltage input

much lower energy consumption. In addition, the disturbance induced by ETE to the particle DEP motion will be lower at the same height in the cylindrical IDE–DEP system compared to the others.

#### 4 Conclusion

In this work, an electrode configuration with interdigitated cylindrical electrodes is suggested. For the first time, the electric field gradient squared was simulated for such a system and compared with plate IDE electrode configuration. The simulation results demonstrate that a cylindrical IDE could provide more homogeneously distributed electric field gradients on the electrode surface and higher electric field gradients than plate IDE above a certain height to the electrodes.

The velocity of resin particle suspended at the surface of demineralized water in a DEP channel mounted by cylindrical IDEs with aspect ratio of 1:2 was theoretically simulated and experimentally measured at different heights of particle to the electrode with experimental error between 0.62 and 5.3 %. In all cases, simulations met experimental results within their standard deviations. This astonishing good agreement indicates that the simulations can be used for reliable predictions of similar systems.

Fluid flow induced by ETE was observed to influence or even determine particle motion. The impact of characteristic length both on ETE fluid flow speed and voltage across medium was demonstrated. The comparison of DEP and ETE velocity, as presented by a ratio of DEP to ETE demonstrated that the DEP velocity is dominant at the height of particle position to the electrode below 6,000  $\mu\text{m}$

in the experimental cylindrical IDE system. The DEP velocities of particle in aqueous medium in cylindrical IDE at different heights of particle position to the electrode were simulated and compared with them in plate IDE and orthogonal electrode configuration. The simulation results demonstrated that the cylindrical IDE could generate more effective DEP effect at identical height compared to the other electrode configurations, and thereby indicating that an identically effective DEP effect with lower energy demand can be expected using cylindrical IDE electrode configuration.

However, to the best of our knowledge, standard microfabrication technologies could not realize a cylindrical form of electrode. For electrode configuration with geometries (electrode size and distance between electrodes) above 100  $\mu\text{m}$ , conventional mechanical processes could be applied by mounting cylindrical electrodes. We suggest micromilling and electroforming processes for fabricating this cylindrical IDE configuration with geometries below 100  $\mu\text{m}$ .

**Acknowledgments** The authors wish to acknowledge German Research Foundation (DFG) for financial support (TH 893/9-1), and Yan Wang thanks China Scholarship Committee (CSC) for financially supporting his contribution.

#### References

- Baune M, Du F, Thöming J (2008) Dielectrophoresis-Bridging the scale in modeling and application. Logos Verlag Berlin GmbH, Berlin
- Cao J, Cheng P, Hong F (2008) A numerical analysis of forces imposed on particles in conventional dielectrophoresis in microchannels with interdigitated electrodes. *J Electrostat* 66:620–626
- Castellanos A, Ramos A, Gonzalez A, Green NG, Morgan H (2003) Electrohydrodynamics and dielectrophoresis in microsystems: scaling laws. *J Phys D Appl Phys* 36:2584–2597
- Cetin B, Li D (2011) Dielectrophoresis in microfluidics technology. *Electrophoresis* 32:2410–2427
- Crews N, Darabi J, Voglewede P, Guo F, Bayoumi A (2007) An analysis of interdigitated electrode geometry for dielectrophoretic particle transport in micro-fluidics. *Sensors Actuators B* 125:672–679
- Du F, Baune M, Thöming J (2007) Insulator-based dielectrophoresis in viscous media—simulation of particle and droplet velocity. *J Electrostat* 65:452–458
- Du F, Baune M, Thöming J (2008) Dielectrophoretic gold particle separation. *Sep Sci Technol* 43(15):3842–3855
- Du F, Hawari A, Baune M, Thöming J (2009) Dielectrophoretically intensified cross-flow membrane filtration. *J Membr Sci* 336:71–78
- Du F, Ciaciuch P, Bohlen S, Wang Y, Baune M, Thöming J (2013) Intensification of cross-flow membrane filtration using dielectrophoresis with a novel electrode configuration. *J Membr Sci* 448:256–261
- Green NG, Morgan H, Milner JJ (1997) Manipulation and trapping of sub-micron bioparticles using dielectrophoresis. *J Biochem Biophys Methods* 35:89–102



- Green NG, Ramos A, Morgan H (2002) Numerical solution of the dielectrophoretic and travelling wave forces for interdigitated electrode arrays using the finite element method. *J Electrostat* 56:235–254
- Jones TB (1995) *Electromechanics of particles*. Cambridge University Press, USA
- Khoshmanesh K, Nahavandi S, Baravandi S, Baratchi S, Mitchell A, Kalantar-zadeh K (2011) Dielectrophoretic platforms for bio-microfluidic systems. *Biosens Bioelectron* 26:1800–1814
- Kumar A, Williams SJ, Wereley ST (2009) Experiments on optoelectrically generated microfluidic vortices. *Microfluid Nanofluid* 6:637–646
- Li X, Chin E, Sun H, Kurup P, Gu Z (2010) Fabrication and integration of metal oxide nanowire sensors using dielectrophoretic assembly and improved post-assembly processing. *Sensors Actuators B Chem* 148:404–412
- Morgan H, Green NG (2003) *AC electrokinetics: colloid and nanoparticles*. Research Studies Press, England
- Morganti E, Collini C, Cunaccia R, Gianfelice A, Odorizi L, Adami A, Lorenzelli L, Jacchetti E, Podesta A, Lenardi C, Milani P (2011) A dielectrophoresis-based microdevice coated with nanostructured TiO<sub>2</sub> for separation of particles and cells. *Microfluid Nanofluid* 10:1211–1221
- Pethig R (2010) Review article—dielectrophoresis: status of the theory, technology, and applications. *Biomicrofluidics* 4:022811
- Pethig R, Markx GH (1997) Applications of dielectrophoresis in biotechnology. *TIBTECH* 15:426
- Pohl HA (1978) *Dielectrophoresis: the behavior of neutral matter in nonuniform Electric Fields*. Cambridge University Press, London
- Ramos A, Morgan H, Green NG, Castellanos A (1998) AC electrokinetics: a review of forces in microelectrode structures. *J Phys D Appl Phys* 31:2340–2353
- Sano N, Matsukura B, Ikeyama Y, Tamon H (2012) Dielectrophoretic particle separator using mesh stacked electrodes and simplified model for multistage separation. *Chem Eng Sci* 84:345–350
- Srivastava SK, Baylon-Cardiel JL, Lapizco-Encinas BH, Minerick AR (2011) A continuous DC-insulator dielectrophoretic sorter of microparticles. *J Chromatogr A* 1218(13):1780–1789
- Thöming J, Du F, Baune M (2006) Dielectrophoretic separation of oil-water-solid dispersions—selectivity and particle velocity. *Fresenius Environ Bull* 15(7):687–691
- Visser DC, Houkema M, Siccama NB, Komen EMJ (2012) Validation of a FLUENT CFD model for hydrogen distribution in a containment. *Nucl Eng Des* 245:161–171
- Weiss B, Hilber W, Gittler P, Jakoby B (2009) Particle separation in alternating-current electro-osmotic micropumps using field-flow fractionation. *Microfluid Nanofluid* 7:191–203